



Article

# Optimizing Contact-Less Magnetoelastic Sensor Design for Detecting Substances Accumulating in Constrained Environments

Ioannis Kalyvas  and Dimitrios Dimogianopoulos \* 

Department of Industrial Design and Production Engineering, University of West Attica, 12241 Athens, Greece; idpe19389276@uniwa.gr

\* Correspondence: dimogian@uniwa.gr

**Abstract:** The optimization of a contact-less magnetoelastic sensing setup designed to detect substances/agents accumulating in its environment is presented. The setup is intended as a custom-built, low-cost yet effective magnetoelastic sensor for pest/bug detection in constrained places (small museums, labs, etc.). It involves a short, thin, and flexible polymer slab in a cantilever arrangement, with a short Metglas<sup>®</sup> 2826 MB magnetoelastic ribbon attached on part of its surface. A mobile phone both supports and supplies low-amplitude vibration to the slab's free end. When vibrating, the magnetoelastic ribbon generates variable magnetic flux, thus inducing voltage in a contact-less manner into a pick-up coil suspended above the ribbon. This voltage carries specific characteristic frequencies of the slab's vibration. If substances/agents accumulate on parts of the (suitably coated) slab surface, its mass distribution and, hence, characteristic frequencies change. Then, simply monitoring shifts of such frequencies in the recorded voltage enables the detection of accumulating substances/agents. The current work uses extensive testing via various vibration profiles and load positions on the slab, for statistically evaluating the sensitivity of the mass detection of the setup. It is shown that, although this custom-built substance/agent detector involves limited (low-cost) hardware and a simplified design, it achieves promising results with respect to its cost.

**Keywords:** magnetoelastic property; Metglas<sup>®</sup>; hypothesis testing; contact-less sensor; vibration analysis; interrogation-free resonator; accumulated substance detection



**Citation:** Kalyvas, I.; Dimogianopoulos, D. Optimizing Contact-Less Magnetoelastic Sensor Design for Detecting Substances Accumulating in Constrained Environments. *Designs* **2024**, *8*, 112. <https://doi.org/10.3390/designs8060112>

Academic Editor: Bhanu Shrestha

Received: 29 September 2024

Revised: 25 October 2024

Accepted: 29 October 2024

Published: 31 October 2024



**Copyright:** © 2024 by the authors. Licensee MDPI, Basel, Switzerland. This article is an open access article distributed under the terms and conditions of the Creative Commons Attribution (CC BY) license (<https://creativecommons.org/licenses/by/4.0/>).

## 1. Introduction

The detection of substances or agents harmful to their environment in sites of difficult or even dangerous (without proper personal protection) access has always been a challenging task. For instance, industrial or research lab facilities may potentially be polluted by chemical/biological substances or infested by agents that prove hazardous when their population becomes significant. On the other hand, sites hosting museum collections and storage facilities or exhibitions of cultural heritage are also included among environments with difficult or constrained access for their technical staff [1–3]. The latter should only access the site when this becomes necessary for rectifying a problem without intervening with the items exhibited or stored. In all aforementioned cases, such sites have to be remotely monitored by means of devices capable of sensing and detecting the accumulation of substances or agents harmful to their environment with humans intervening only when absolutely required.

Magnetoelasticity or magnetostriction is an interesting property exhibited by some (ferromagnetic) materials, which can be useful for developing remotely operated sensing and detection setups. According to this property, specific materials modify their shape due to external varying magnetic fields but also emit magnetic flux when they suffer external variable load [4–6]. Then, if strips made of magnetoelastic material are suitably mounted (for instance, clamped on both sides) inside a space to be monitored, and an external variable

magnetic field is imposed, the strip will experience (subtle) longitudinal shape changes. Due to the strip being clamped, these changes will result in the strip vibrating, with the vibration dynamics influenced by the external magnetic field and the strip's dimensions and mass distribution. Hence, if substances such as biological agents [7,8], air pollutants [9], volatile organic compounds [10], H<sub>2</sub>O [11–13], or H<sub>2</sub>O<sub>2</sub> [14] start accumulating on the strip surface, its mass distribution along with its vibration dynamics will change. Note that this substance accumulation on a precise part of the strip is facilitated by means of specific coatings applied on the strip. Then, shifted resonant frequencies (detected by remotely monitoring the vibrating strip's dynamics) indicate a significant accumulation of substances on the strip and, consequently, in the monitored site.

The principle for remote sensing and detection of (substance/agent-induced) changes based on monitoring the vibration dynamics of a magnetoelastic strip has given rise to various different setups. One main class involves setups designed so that the magnetoelastic strip (or other element) vibrates at its resonant frequency due to an interrogation coil suitably fed by an electrical current to provide a variable magnetic flux to the strip, without bearing contact with it. Then, another coil (referred to as the pick-up coil) is suspended above the strip (again without being in contact with it) and transforms the magnetic flux emitted from the vibrating strip into voltage. The latter may then be recorded and uploaded to a remote host in order to monitor any frequency shifts indicating mass (i.e., substance) accumulation. This two-coil approach is referred to as the active design [15] and is quite sensitive to mass accumulation on the surface of the magnetoelastic strip. Schemes such as those presented in [7–14] follow this approach, which has been extensively studied (in [8], for instance) both experimentally and theoretically in terms of detection sensitivity and quality factor (related to the sharpness of sensor resonance). Further improvements on these two fronts are possible by choosing to use a strip based on its Young's modulus and  $\Delta E$  effect characteristics [16], its length-to-width ratio [16–18], or even its shape, with hour-glass [19] or rhomboid forms [20,21] considered as more effective. In [22], a comprehensive presentation and analysis of relevant designs may be found.

Another class of setups is designed to use mechanical excitation from devices or structures upon which the strip is mounted, for setting the strip into vibration (along with the device/structure), without requiring an interrogation coil. The vibrating strip then emits magnetic flux, which induces voltage into a pick-up coil suspended above the strip. Analyzing the voltage signal's spectral characteristics allows for monitoring frequency shifts either due to mass deposition on the structure surface [23,24], from any changes to the structure's frequency of mechanical vibration [24], or even from structural faults affecting the device/structure upon which the strip is fixed [25–30]. The last point illustrates the fact that the single-coil setup (or passive design, as it is also referred to in [15]) is well suited to fault detection and isolation (FDI) tasks for structures and/or systems. Note that, sometimes, setups involving magnetoelastic components as parts of a vibrating structure and aiming at estimating its spectral characteristics make use of a DC-fed interrogation coil. This induces bias to the magnetic flux produced by the magnetoelastic component and helps to achieve better results [30,31]. This remark also indirectly indicates the main weakness of the passive setup: the resulting magnetic flux is significantly weaker than that produced in active setups. On the other hand, passive setups have lower operational costs and are far simpler in terms of electrical or electronic circuits and general hardware used. Ultimately, although signals obtained by passive setups are noisy, faults/failures impacting the dynamics of the underlying structure (or machinery) are, indeed, detectable in the frequency content of these signals [25–27].

The current work followed the passive design approach by introducing a minimal (in terms of hardware), simple, and cost effective to custom build and operate setup, which, nonetheless, performed well with respect to its cost. The basic layout was first introduced in [23], even though this was merely a proof-of-concept study, without any evaluation of its potential performance and effectiveness. The latter was the objective of

the current study, which employed extended testing along with a statistical validation of results to evaluate its performance and identify its operational limits. Briefly, a short, thin, and flexible polymer slab was fixed in a cantilever arrangement, with a short Metglas<sup>®</sup> 2826 MB magnetoelastic ribbon attached on its clamped end. A mobile phone both supported and supplied a low-amplitude vibration to the free end. Under vibration, magnetic flux emitted by the magnetoelastic ribbon induced voltage in a pick-up coil suspended above the ribbon. This voltage carried specific characteristic frequencies of the slab's vibration. If substances/agents accumulated on parts of the (suitably coated) slab surface, its mass distribution and, hence, characteristic frequencies changed. Then, simply monitoring shifts of such frequencies in the recorded voltage enabled the detection of accumulating substances/agents. Note that, to the best of the authors' knowledge, a similar setup for a pest or bug detector has not been proposed in the literature. Therefore, no direct comparison was possible other than with devices detecting various harmful biological agents/substances, which usually operate on the two-coil design principle [7–14]. These are quite more complex to build and operate, thus, quite more expensive. Care, also, had to be taken when cleaning/replacing the magnetoelastic element, in order to retain its high effectiveness in detecting H<sub>2</sub>O, H<sub>2</sub>O<sub>2</sub>, or specific biological agents. The paper is organized as follows: After a brief introduction in Section 1, the setup is presented in Section 2 both at its nominal state of operation and at its optimization phase. Section 3 presents the results of testing, along with their statistical interpretation, which defines the envelope of effective operation of the setup, whereas Section 4 provides a brief discussion with interesting remarks on the findings of Section 3. Finally, Section 5 presents some concluding remarks and future work directions.

## 2. Materials and Methods

### 2.1. Nominal State of Operation

The setup, shown in Figure 1a,b, was initially proposed in [23], although, for this work, it was suitably modified due to component availability and/or attempts to improve operational effectiveness. The basic component was a thin polymer slab measuring 100 × 30 × 0.8 mm with a Metglas<sup>®</sup> 2826 MB ribbon of 25 × 5 mm centered in the lateral direction on the slab surface and fixed with cyanoacrylic glue (see Figure 1b). Obviously, the setup is scalable by the user according to the available space on site. The use of Metglas<sup>®</sup> 2826 MB<sup>®</sup> (or equivalent) ribbons was because these may be found at a relatively moderate price and are available off the shelf via the internet. Better performing solutions (magnetolectric laminates, for instance [32]) may be used instead, but a 25 mm long Metglas<sup>®</sup> 2826 MB<sup>®</sup> ribbon is probably a more cost-effective solution for a small lab or a museum lab or small museum wishing to obtain pest detection results without investing in infrastructure. For instance, monitoring pest occurrence in a small museum collection following integrated pest management (IPM) procedures [2,3] would require a setup of limited size placed in as discreet a location as possible. The slab end, upon which the Metglas<sup>®</sup> 2826 MB ribbon was attached, was fixed as a cantilever via a clamp or a vice. The opposite end received excitation by means of a low-amplitude vibration signal input. Following the magnetoelastic principle [4–6], the vibrating ribbon produced magnetic flux, which varied in accordance with the vibration dynamics of the slab. The changing magnetic flux, in turn, induced voltage in a low-cost pick-up coil (Vishay IWAS) placed 15 mm above the ribbon, i.e., in a contact-less manner (see Figure 1b). Frequency analysis of the voltage allowed for detecting changes (mainly frequency shifts) in slab dynamics due to mass accumulated on its surface.

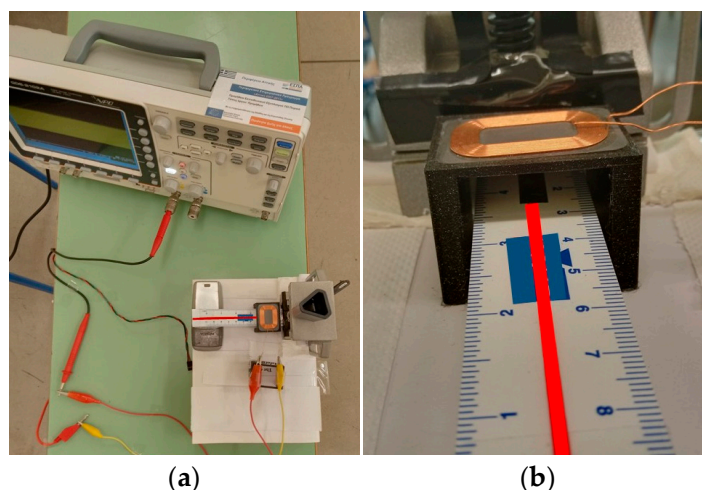


**Figure 1.** Components of the setup: (a) the polymer slab clamped on the right and supported by a feature phone on the left, with the pick-up coil near the clamp; (b) detail of the clamped end with the pick-up coil placed on a supporting base above the Metglas<sup>®</sup> ribbon fixed at the end of red line.

Due to the high flexibility of the slab, its free end required it to be supported in order to be level with the clamped end and, hence, close to the nominal configuration of fixed-pinned beams as treated, for instance, in [33]. At the same time, the supported end should vibrate at a specific optimal frequency and profile (see Section 2.2). Hence, a cellular phone of suitable thickness can be used both as a support and as an exciter that provides vibration to the slab, whenever this is required by the user. For this work, an old low-cost feature phone was used (see Figure 1a), which provided an excitation profile roughly similar to the one identified as most effective (see Sections 2.2 and 3.1), and it only required recharging once a week. The voltage received by the pick-up coil was recorded by a conventional oscilloscope, without requiring filtering (and, hence, the use of relevant circuit/hardware) before being processed. Alternatively, a standard smartphone could be used, which should allow for a two-fold evolution of the setup, as follows:

- First, the signal produced by the coil could be recorded (and uploaded to a remote host for further analysis) by the smartphone via custom-made applications. Hence, an oscilloscope would no longer be necessary, whereas automated “over-the-air” operation would be readily obtainable.
- Second, different vibration profiles could be suitably defined by the user according to the findings in Section 3.1, again via custom-made applications.

On top of the already minimal complexity (no interrogation coil and no voltage filtering and associated hardware/circuitry), both developments should result in a considerably more versatile setup. It should make for a low-cost, simple, custom-made setup for monitoring confined or hard to access environments (a small museum collection or storage facilities, small labs, etc.). Indeed, the total cost is largely proportional to the value of the mobile phone. The pick-up coil, a 25 mm long Metglas 2826 MB<sup>®</sup> ribbon, the clamp with its support, and the digital acquisition device (in this case, an oscilloscope) cost less than a low-cost smartphone. If a smartphone is used, then one may use it both as an excitation and acquisition device, by means of specific applications. The power consumption of the setup is that of a mobile (smart)phone receiving calls in its vibration-only mode several times a day (and idling during the rest of it), whereas range, durability, and size mainly depend on the particular phone used.

## 2.2. Testing Conditions: Setup Optimization

The previous subsection regarded the *nominal* state of operation of the setup, meaning that the setup presented supposed that the slab vibrated due to an optimally chosen signal and substances/agents were accumulating on the most sensitive part of the surface, so

that best detection performance could be achieved. Nonetheless, identifying these optimal settings was the principal objective of the current study, and this imposed considerable testing using specific technical solutions and methods. Figure 2 presents the setup as modified for optimization testing. The cellular phone was removed, with a module (designated as part A) involving a small vibration motor and the associated circuit taking its place and supporting the free end of the slab. The vibration module (in the form of a tab) was similar to those used in cellular phones but could be driven by the user to produce specific vibration profiles. Note that in Figure 2, the vibration module is already in place, with the module marked with an A presented (and shown in the inset) simply for clarity. In the current study, the vibration module A was driven via an Arduino-Uno Atmega328 microprocessor (designated as part B in Figure 2) connected to a portable computer, which, via suitable programming, may act as function generator. Pulse signals of either constant user-defined frequency values or frequency sweeps within a user-defined range may be obtained via the microprocessor.

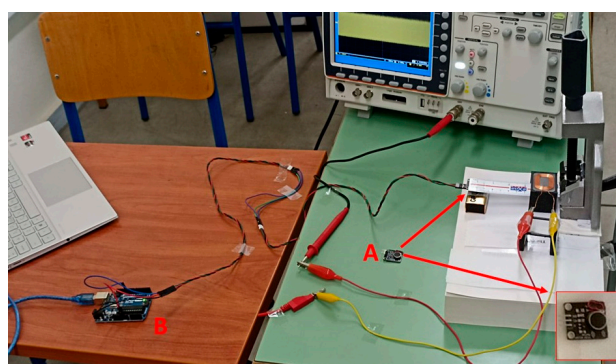


**Figure 2.** Evaluating the setup for sensitivity and detection effectiveness by replacing feature phone with vibration module A (see inset) fixed under the slab (see short arrow) and driven by an Arduino-Uno microcontroller B, connected to the portable computer on the left.

A previous study [24] demonstrated that long, thin, flexible polymer beams with magnetoelastic ribbons attached to their surface can actually provide sensing information, which allows for estimating the vibration frequency level. Based on this fact, the current study went a step further in that it identified the vibration profile, which maximized the sensing properties of the polymer slab before attempting to use these properties for detection purposes. Therefore, an initial set of test runs involved a series of triangular pulses (as in [24]) vibrating the slab at (constant for each test run) values of 30, 60, 90, 120, 150, and 180Hz. Additionally, a series of pulses sweeping the frequency range between 30 and 180Hz were also tested. Note that testing at frequencies over 180Hz was also attempted, but occasional problems with the vibration module were encountered. All profiles were used for vibration testing on two different occasions (days). As will be explained in Section 3, performing the same tests on different days allowed for reliably identifying critical frequency regions where sensing properties of the slab were evident. Hereafter, such regions are referred to as *principal activity regions*. By definition, prominent frequency peaks in principal activity regions must be created by all vibration profiles for a slab vibrating without substances/agents accumulating on its surface. Note that in a similar context, [25] confirmed via finite element analysis that such frequency peaks were close to specific characteristic frequencies of the setup. Then, specific vibration profiles, which lead to the highest peaks inside each principal activity region, may be identified, meaning that best (i.e., optimal) and worst-case vibration profiles are readily designed.

At a later stage, the optimally selected vibration profiles were used to monitor the principal activity regions for frequency shifting due to the accumulation of substances/agents on the slab's surface. Two issues were important, at this stage, and both were related to the

sensitivity of detecting substances/agents accumulating on the slab. The first sensitivity issue was related to finding slab locations where accumulating substances/agents led to the most evident frequency shifts inside the considered principal activity regions. Therefore, three different locations were examined on the slab, namely, at 4, 6, and 8 cm away from the clamped end, as presented in Figure 3. These locations are referred to as W4, W6, and W8, respectively. Note that the Metglas<sup>®</sup> ribbon was fixed right after the clamp, meaning that W4 was the most accessible point close to the Metglas<sup>®</sup> ribbon's end that could be used for detection purposes. Recall that the ribbon was 25 mm long, meaning that its end was still 15 mm away from W4. This choice of the W4 location was purely due to practical reasons: If substances/agents-to-be-detected are pests or bugs, then a special pest/bug-attracting coating should be applied on the slab surface. Removing the captured bugs could be a problem, if part of this coating is applied by mistake under the coil support or on the ribbon. For the same reason, the coil was placed at a distance of 15 mm above the slab surface, even though [24] demonstrated that, as this distance decreases, results in terms of frequency peaks inside the principal activity regions become more consistent. Location W6 was slightly off the middle of the slab, whereas location W8 was practically near the vibration module. The latter covered the part between 8 and 10 cm of the slab. Note that any pest/bug-attracting coating should not be applied over the entire slab surface but rather on that location (W4, W6, and W8) that offers the best sensitivity in terms of frequency shifts inside the principal activity regions. Note, also, that detection effectiveness is not linearly proportional to the volume of a coated part on the slab surface. In other words, a "limited" area of accumulated pest means that a point (instead of a uniform) load is applied onto the slab, which is favorable to reduced detection times.

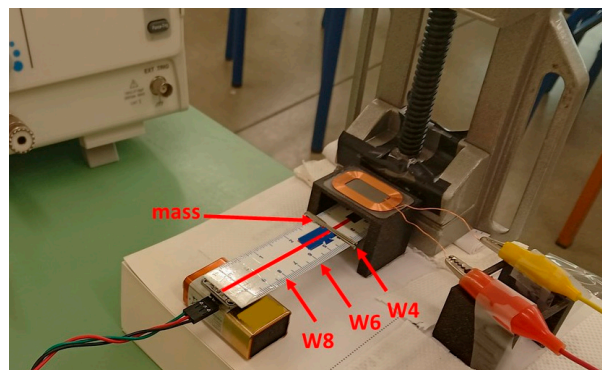


**Figure 3.** Locations where a mass of 0.46 g is placed during testing: location W4, the closest possible to the ribbon (which lies under the coil-supporting base); location W6 near the middle; location W8 right in front of vibration module and its supporting base.

The second sensitivity issue was related to defining the potential value of the mass of the accumulating substances/agents to be detected, which should be as low as possible. A past study [23] indicated that masses as low as 0.5 g could be detected, and this was the starting point of the current study. A group of needles stacked together and weighing in total 0.46 g was used for testing at locations W4, W6, and W8 (see Figure 3) under different vibration scenarios involving both optimal and worst-case vibration profiles, in the sense explained in previous paragraphs. The choice to vibrate the slab at both optimal and worst-case vibration profiles ultimately led to the global assessment of performance limitations of the setup, both in positive and negative terms.

Addressing both sensitivity issues implies that a number of test runs at unloaded (no mass on slab surface) and loaded (with 0.46 g of needles) configurations for locations W4, W6, and W8 should have been carried out. The resulting signals were recorded and, via frequency analysis plots (via fast Fourier transform (FFT)), datasets including frequency values associated to peaks should have been formed for cases of testing with unloaded slabs as well as cases of slabs with loads at W4, W6, and W8. Forming such datasets for each

principal activity region and comparing them by means of statistical hypothesis testing procedures allows for examining whether datasets corresponding to loaded slabs at a specific location (W4, W6, or W8) are meaningfully different in a statistical sense compared with datasets resulting from unloaded slabs. Such statistical evaluations provide reliable evidence as to whether frequency peaks from loaded slabs are shifted with respect to peaks from unloaded slab inside each principal activity region.

Furthermore, the results of such statistical evaluations take into account the inherent uncertainty of the decision-making process. In fact, comparing two or more datasets may be seen as a problem of checking whether data in all sets follow the same statistical distribution or not. The hypothesis testing problem may, hence, admit the following form, as follows:

$$\begin{aligned} H_0: & \text{Data (frequency values) in both (or all) sets follow a similar distribution.} \\ H_1: & \text{Data (frequency values) in both (or all) sets follow different distributions.} \end{aligned} \quad (1)$$

In (1),  $H_0$  is referred to as the null hypothesis, whereas  $H_1$  is the alternative hypothesis. In essence, data in each set may follow any distribution and, while statistical checks to decide whether data are normally distributed exist, they are not very useful when the amount of data values in each set is limited. Hence, given that there is no indication that data in the frequency values sets follow normal distribution, non-parametric statistical tests are suitable for choosing between null and alternative hypotheses in (1) at a given risk level  $\alpha$ . The latter is the probability of rejecting  $H_0$ , even though it is true and is usually selected equal to 0.05. In other words, rejecting  $H_0$  at  $\alpha = 0.05$  means that there is only a 5% probability of uncertainty (or risk) to be mistaken and accept that “data of sets under comparison follow different distributions”, while in reality they do not. Typical non-parametric statistical tests are the Kolmogorov–Smirnov two-sample test and the Kruskal–Wallis test [34,35]. The Kolmogorov–Smirnov two-sample test is used for solving hypothesis problems as in (1), when comparisons between only two datasets are considered. The null hypothesis is accepted (or rejected), using the distance between empirical distributions of data for each set, with this distance estimated on the basis of the available data. On the other hand, the Kruskal–Wallis test may be used with two or more sets of data [34–36] and assesses whether data in sets under consideration follow similar distributions. If these distributions have similar shapes, then the Kruskal–Wallis test accepts (or rejects) the null hypothesis based on whether medians of all groups are sufficiently (in some statistical sense) close [34]. The important detail is that the Kruskal–Wallis test can even be used with sets containing as low as 6 data values each [36]. For instance, cases of using the Kruskal–Wallis test with groups containing a very limited number of data values are presented in [34,35]. On the other hand, when two datasets (involving  $n_1$  and  $n_2$  data values, respectively) should be compared, the Kolmogorov–Smirnov test is believed to give reasonably accurate results if  $[(n_1 \times n_2)/(n_1 + n_2)] \geq 4$  [37], which could be a matter of concern in the present case (see Section 3.2). These characteristics motivated the choice of Kruskal–Wallis test for solving the hypothesis testing problem (1), as presented in Section 3.1. The Kruskal–Wallis test may be found in software packages such as SPSS® or MATLAB® (with the latter used in this study), which instantly provide the probability value (referred to as  $p$ -value) for evaluating the evidence against the null hypothesis. A low  $p$ -value means that there is significant evidence against accepting the null hypothesis. The  $p$ -value also provides a means for quantifying how much risk (uncertainty) is involved when two (or more) datasets (frequency peak values in the case examined) are considered to overlap. Then a large  $p$ -value would state that the sets considered should almost surely overlap, meaning that frequency shifts are not significant.

### 3. Results

As stated in Section 2, the experimental testing aimed at obtaining a two-fold assessment of the setup, as follows:

- First, the principal activity regions inside the frequency range where sensing characteristics are evident should be determined for a slab vibrating at an unloaded configuration. Various vibration profiles at different frequencies (constant as well as frequency sweeps) were created (see Section 2.2) and used for slab excitation. Frequency analysis of the resulting voltage (as provided by the pick-up coil) was used to define the principal activity regions where frequency peaks were most prominent for all vibration profiles tested. Additionally, testing was performed at two different days (occasions) in order to retain only principal activity regions common to both days. Hence, frequency regions with peaks from transient phenomena or electromagnetic noise were avoided. This task is presented in Section 3.1.
- Second, once a clear decision on the most (and the least) effective vibration profile was made, the effectiveness to detect frequency shifts (from mass accumulation on W4, W6, or W8 slab locations) should be evaluated. This evaluation involves the use of Kruskal–Wallis statistical hypothesis tests and will be presented in Section 3.2.

In all test runs, the slab vibrated during several seconds and the voltage from the pick-up coil was recorded at 2 MHz. Each time, frequency analysis plots using FFT were created using signal sequences of  $2 \times 10^6$  samples.

### 3.1. Sensitivity of Sensing Characteristics Versus Vibration Profiles

Initially, test runs using triangular pulses of 30, 60, 90, 120, 150, and 180Hz to vibrate the slab were conducted. Subsequently, a series of pulses at frequency sweeps between 30 and 180Hz were also used to vibrate the slab. The same testing protocol was applied during two different days in order to isolate principal activity regions common to both days. Figure 4 presents the results of the second day of testing, whereas in Table 1, the three most significant principal activity regions are listed for each day. Obviously, two regions were common to both days, namely, that around 5300–5400Hz (first principal activity region) and another around 2600–2700Hz (second principal activity region). The region around 5400Hz was considered as the most significant (and, hence, referred to as the first principal activity region) because frequency peaks therein had up to 10 times larger amplitude than their counterparts found in the region around 2700Hz (see, for instance, peaks created by frequency sweep excitation in Figure 4).

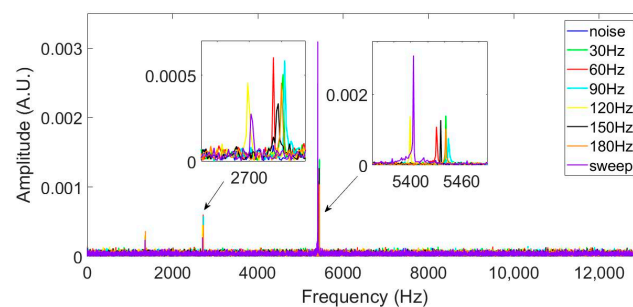


**Figure 4.** Frequency plots of recorded voltage (as provided by the pick-up coil) following testing using various vibration profiles for evaluating sensitivity, with first (around 5400Hz) and second (around 2700Hz) principal activity regions shown in insets.

**Table 1.** Testing days and the three most significant principal activity regions.

Day of Testing	First Principal Activity Region (Hz) <sup>1</sup>	Second Principal Activity Region (Hz) <sup>1</sup>	Third Principal Activity Region (Hz) <sup>1</sup>
#1	5300	2600	36,000
#2	5400	2700	1350

<sup>1</sup> Region  $\pm 80$ Hz approximately around indicated value.



There were other regions where peaks were prominent but corresponded to signals created by only one or two vibration profiles. For instance, around 200 KHz, one may notice a large peak corresponding to signal resulting from vibrating the slab at 30Hz on both days. It is critical that a principal activity region includes peaks corresponding to all vibration profiles tested, since the most as well as the least effective vibration profile (out of all tested) should be designated at each principal activity region. Another remark regards the inclusion of a signal referred to as noise in Figure 4. In fact, the first series of test runs were conducted without vibrating the slab, meaning that the pick-up coil provided a signal corresponding to (mostly electromagnetic) ambient noise. Obviously, this noise should not result in frequency peaks inside principal activity regions, since, in those regions, only information resulting from the vibration dynamics of the slab should be present.

In order to check whether the amplitude of frequency peaks of signals created by any excitation profile could be comparable to those of noise, additional testing was carried out. Five noise sequences were recorded and, again, five test runs for each excitation profile were carried out. Frequency peaks and amplitudes were computed (via FFT) for each set of five signals. Then, error bar-like plots indicating amplitude dispersion for each set of signals due to an excitation profile versus dispersion from signals due to noise were created for both principal activity regions in Figure 5a,b. No overlap was noted, meaning that when the slab vibrated due to external excitation, its response was visible through noise inside both principal activity regions.

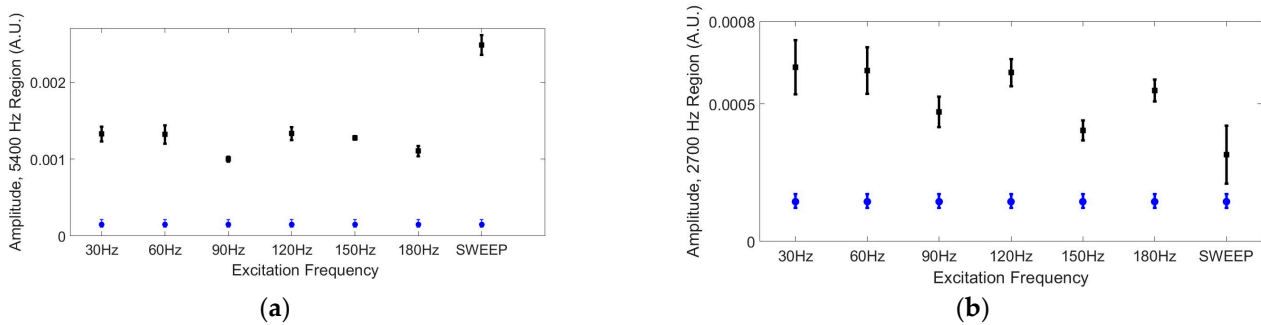


**Figure 5.** Amplitude dispersion of frequency peaks of signals created from each excitation profile (in black) versus noise (in blue): (a) in the first principal activity region; (b) in the second principal activity region.

Note that, inside each principal activity region, the most prominent frequency peaks did not systematically result from the same vibration profile. When more than one principal activity regions are considered, a rule designating the most effective vibration profile must be defined. Considering that, in terms of sensing, the vibration profile creating the highest peak magnitude in a region was the most effective, a rule was formulated, as follows.

- Inside each principal activity region, select the vibration profile resulting in the highest peak magnitude, namely,  $A_{max}$ .
- For each of the remaining vibration profiles, compute the index  $i_x$  corresponding to its relative difference with respect to the highest peak magnitude, namely,

$$i_x = (A_x - A_{max}) / A_{max} \tag{2}$$

with  $x$  designating the vibration profile examined (30, 60, 90, 120, 150, 180Hz or sweep 30–180Hz).

- For each vibration profile  $x$ , compute:

$$I_x = \sum_{k=1}^n i_x \tag{3}$$

where  $n$  is the number of principal activity regions.

Vibration profiles with the lowest values of  $I_x$  should qualify as most effective since they resulted in high peak magnitudes in all principal activity regions. Figure 6 presents a bar chart based on the values of  $I_x$  following testing with all vibration profiles during two days. Note that, for reasons of clarity, values for  $I_x$  are shown for the first [i.e.,  $n = 1$  in (3)] and both [ $n = 2$  in (3)] principal activity regions. One may, hence, note that several vibration profiles perform better when only considering the first principal activity region (brown bars), with that corresponding to the frequency sweep being the best ( $i_x = 0$ ), followed by the profile of 30Hz. Obviously the best overall effectiveness was demonstrated by the profile corresponding to the frequency sweep (green bars). The worst-case profile had to be either that corresponding to the series of triangular vibration pulses at 150 or 180Hz. The profile of 150Hz had an equally poor performance in both principal activity regions, whereas that of 180Hz behaved badly inside the first region and slightly better inside the second one. After much thought, the vibration profile at 180Hz was selected as the worst-case scenario in terms of sensitivity. This is because it featured notably poorer effectiveness inside the (most significant) first principal activity region, where peak magnitudes were higher than in every other region of the frequency band. Note that it seemed quite surprising that the two vibration profiles with the highest frequencies were candidates for being less effective in terms of sensing results. This issue will be further discussed in Section 4. It is important to test the most and the least effective vibration profiles, because this should offer a global view of the performance limits of the proposed setup in terms of the detection of mass accumulating on the slab surface, as will be explained in Section 3.2.

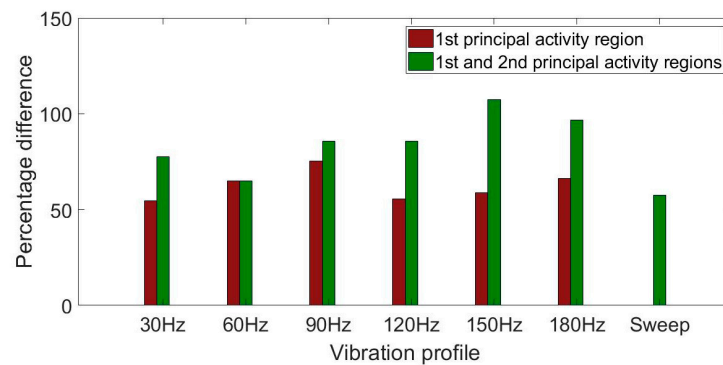


**Figure 6.** Values for  $I_x$  criterion in (3) (green bars) for all vibration profiles in both principal activity regions (also value for  $I_x$  in the first principal activity region with brown bars, for comparative purposes): lower bars indicate better sensing obtained from the corresponding vibration profile.

### 3.2. Sensitivity of Mass Detection Versus Magnitude/Position on the Slab Surface

Once the best and worst-case configurations have been defined, the assessment of mass detection effectiveness with respect to mass position on the slab surface must be carried out. For this purpose, test runs at unloaded (no mass on slab surface) or loaded configurations (mass at slab locations W4, W6, or W8) were performed and are reported in Table 2. The notation of the configuration for each test run indicates the vibration profile used for conducting the runs. Notations involve the frequency value at which the run was conducted (30–180Hz or sweep) and the mass location during the run (W4, W6, W8, or no mass reference) whereas  $j$  indicates the current test run number at this particular configuration. Given that 10 test runs per configuration were conducted,  $j$  admits values between 1 and 10. For instance, 180HzW4,3 indicates results from the third run conducted by vibrating the slab at 180Hz, with a mass (of 0.46 g) at location W4. On the other hand, 180Hz,3 indicates results from the third run conducted by vibrating the slab at 180Hz without load on its surface.

**Table 2.** Test runs and associated configurations, with statistical hypothesis testing results using Kruskal-Wallis test.

Configuration for Each Dataset $j = 1, \dots, 10$	$p$ -Value: Accepted Hypothesis First Principal Activity Region 5300–5400Hz	$p$ -Value: Accepted Hypothesis Second Principal Activity Region 2600–2700Hz
180Hz $_j$	$1-H_0$	$1-H_0$
180HzW4 $_j$	0.020507— $H_1$	0.020459— $H_1$
180HzW6 $_j$	0.00027618— $H_1$	0.00030979— $H_1$
180HzW8 $_j$	0.00086503— $H_1$	0.000838— $H_1$
sweep $_j$	$1-H_0$	$1-H_0$
sweepW4 $_j$	0.00015262— $H_1$	0.00015174— $H_1$
sweepW6 $_j$	0.00015705— $H_1$	0.00015527— $H_1$
sweepW8 $_j$	0.13987— $H_0$	0.11106— $H_0$

When a series of 10 runs at a given vibration profile was completed both at loaded and unloaded configurations, the frequency values of peaks inside the first and second principal activity regions were stored. Thus, for each principal activity region, two datasets per configuration were formed: one set with 10 frequency values corresponding to the unloaded slab and another with 10 frequency values corresponding to a slab loaded at one of the designated locations (W4, W6, or W8). Then, the Kruskal–Wallis test was used for evaluating whether data in these sets followed the same distribution (i.e., accepting hypothesis  $H_0$ ) or not (i.e., accepting hypothesis  $H_1$ ). Accepting  $H_1$  means that the set of peak frequencies from testing at an unloaded configuration did not overlap with that formed by peak frequencies from testing at a loaded configuration, at  $\alpha = 0.05$  risk level. In other words, accepting  $H_1$  means that testing with loaded slabs resulted in shifted frequency peaks with respect to those exhibited when testing with unloaded slabs. Results for  $p$ -values and the accepted hypotheses inside each principal activity region are shown in Table 2. For instance, if the  $p$ -value was equal to  $0.020507 < 0.05$  (third row, second column), then comparing the frequency set from tests at a “180HzW4 $_j$ ” configuration (load at W4, constant vibration of 180Hz) to the set from tests at a “180Hz $_j$ ” configuration (no load, constant vibration of 180Hz) resulted in the two sets not being not similar ( $H_1$  accepted) at a  $\alpha = 0.05$  risk level, and by some margin. Again, if the  $p$ -value was equal to  $0.00015262 < 0.05$  (seventh row, second column), that indicated that the frequency set from tests at a “sweepW4 $_j$ ” configuration was not similar to that from tests at a “sweep $_j$ ” configuration at  $\alpha = 0.05$  risk level, and by a wider margin than before. Note that if the Kolmogorov–Smirnov (instead of Kruskal–Wallis) test is used, one must make sure that the two sets contain sufficient data values ( $n_1$  and  $n_2$ , respectively) so that the index  $[(n_1 \times n_2)/(n_1 + n_2)] \geq 4$  (see Section 2.2). In the current case, with  $n_1 = n_2 = 10$ , the index admitted a value equal to 5; hence, results could be acceptable, but only just.

Furthermore, frequency plots in Figures 7–12 exhibit the frequency shifting phenomena evaluated in Table 2 via the Kruskal–Wallis test and the corresponding  $p$ -values. An examination of Figures 7–12 (particularly the plots showing peak dispersion in both principal activity regions) is important in order to associate  $p$ -values found in Table 2 with the level of overlap between the corresponding frequency sets. Note that, for cases with important frequency shifts such as in Figure 10 (“sweep $_j$ ” versus “sweepW4 $_j$ ” configuration), very low  $p$ -values (equal to 0.00015262) were obtained. On the other hand, a  $p$ -value equal to 0.020507, which is significantly lower than 0.05, did not exclude a small overlap between frequency sets in Figure 7 (“180HzW4 $_j$ ” versus “180Hz $_j$ ” configuration). Nonetheless, the majority of test runs with load at W4 did exhibit shifted frequencies when the slab vibrated at 180Hz, with respect to test runs conducted without load. Note also that low  $p$ -values ultimately indicate shifting of frequency peaks when the slab was loaded but did not indicate the direction. For instance, results in the 4th–5th rows of Table 2 and

Figures 8 and 9 show that frequencies shifted to higher values when the vibrating slab was loaded, yet  $p$ -values only indicated that frequency shifts existed. This result will be discussed in Section 4.

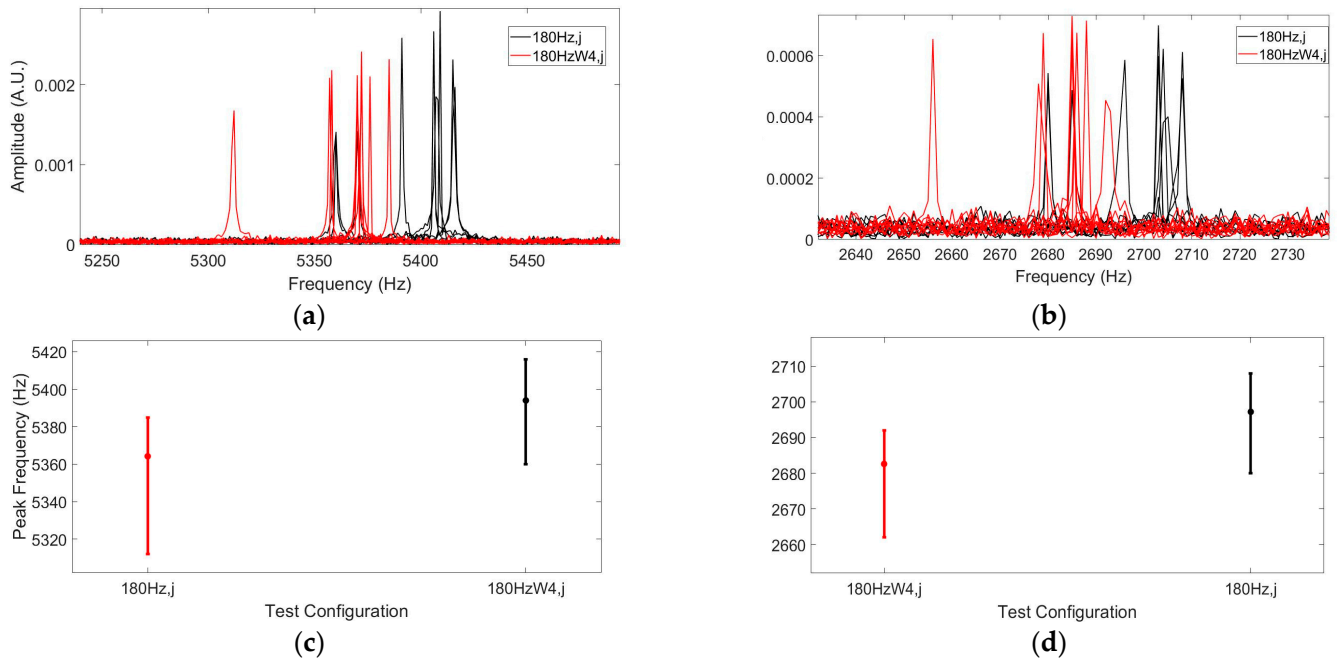


**Figure 7.** Frequency plots of voltage signals obtained via the pick-up coil from a slab vibrating due to excitation at 180Hz without and with mass at W4: (a) peaks in first principal activity region; (b) peaks in second principal activity region; (c) peak dispersion for both configurations in first principal activity region; (d) peak dispersion for both configurations in first principal activity region.

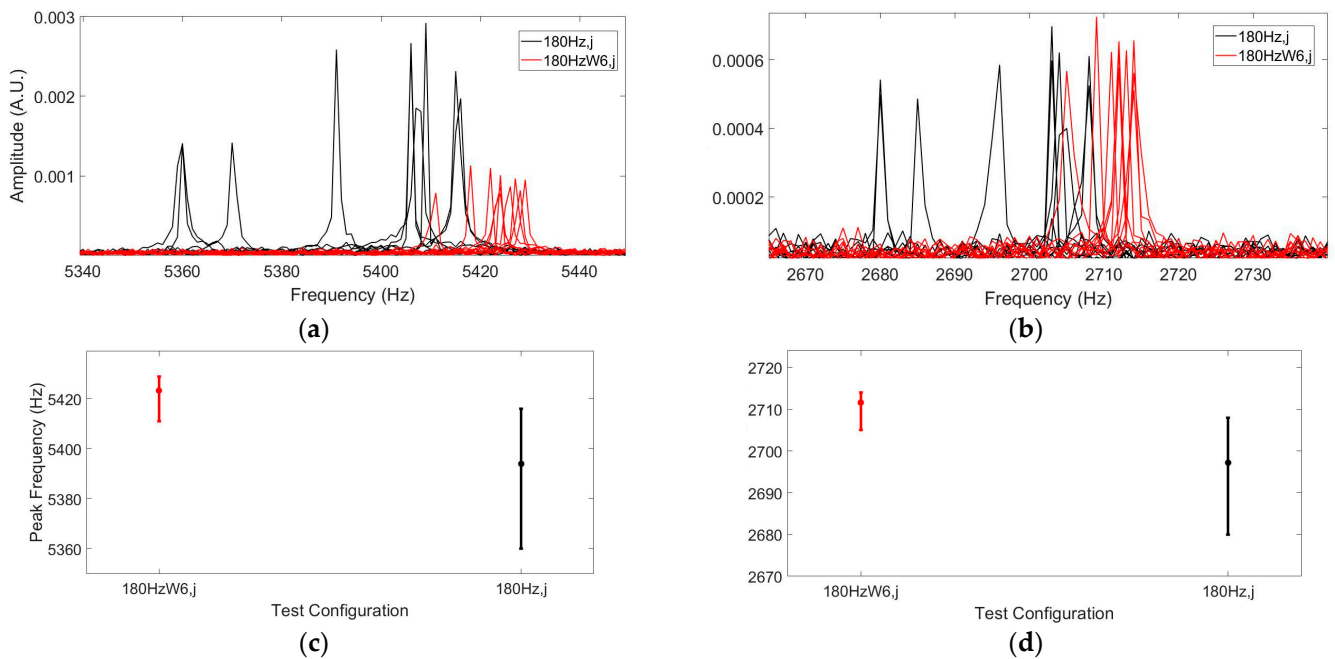


**Figure 8.** Frequency plots of voltage signals obtained via the pick-up coil from a slab vibrating due to excitation at 180Hz without and with mass at W6: (a) peaks in first principal activity region; (b) peaks in second principal activity region; (c) peak dispersion for both configurations in first principal activity region; (d) peak dispersion for both configurations in first principal activity region.

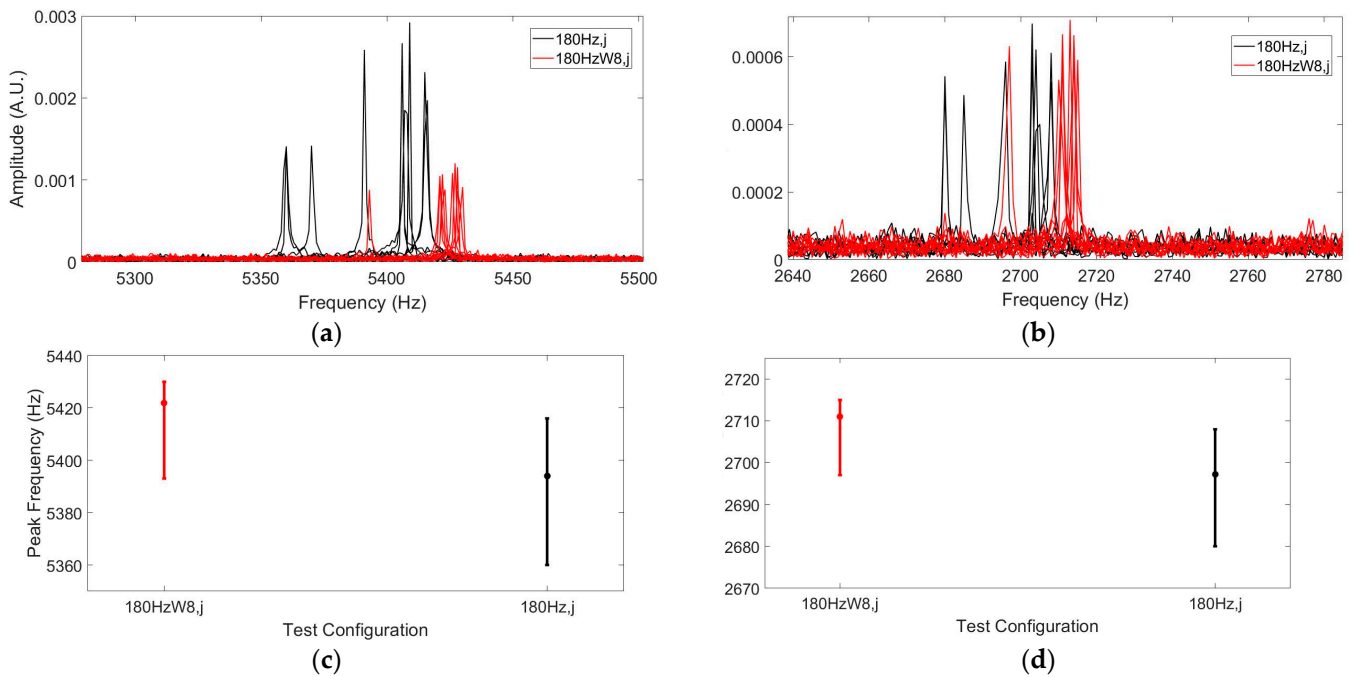


**Figure 9.** Frequency plots of voltage signals obtained via the pick-up coil from a slab vibrating due to excitation at 180Hz without and with mass at W8: (a) peaks in first principal activity region; (b) peaks in second principal activity region; (c) peak dispersion for both configurations in first principal activity region; (d) peak dispersion for both configurations in first principal activity region.

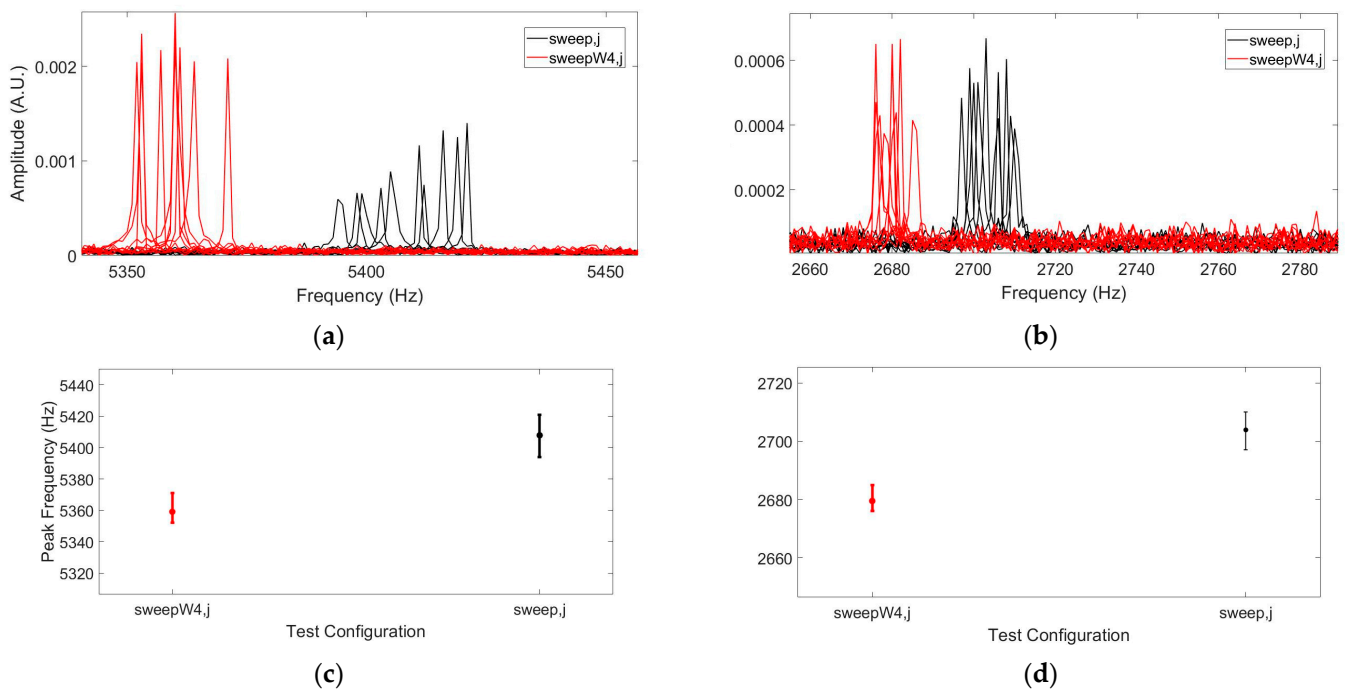


**Figure 10.** Frequency plots of voltage signals obtained via the pick-up coil from a slab vibrating due to frequency sweep excitation without and with mass at W4: (a) peaks in first principal activity region; (b) peaks in second principal activity region; (c) peak dispersion for both configurations in first principal activity region; (d) peak dispersion for both configurations in first principal activity region.

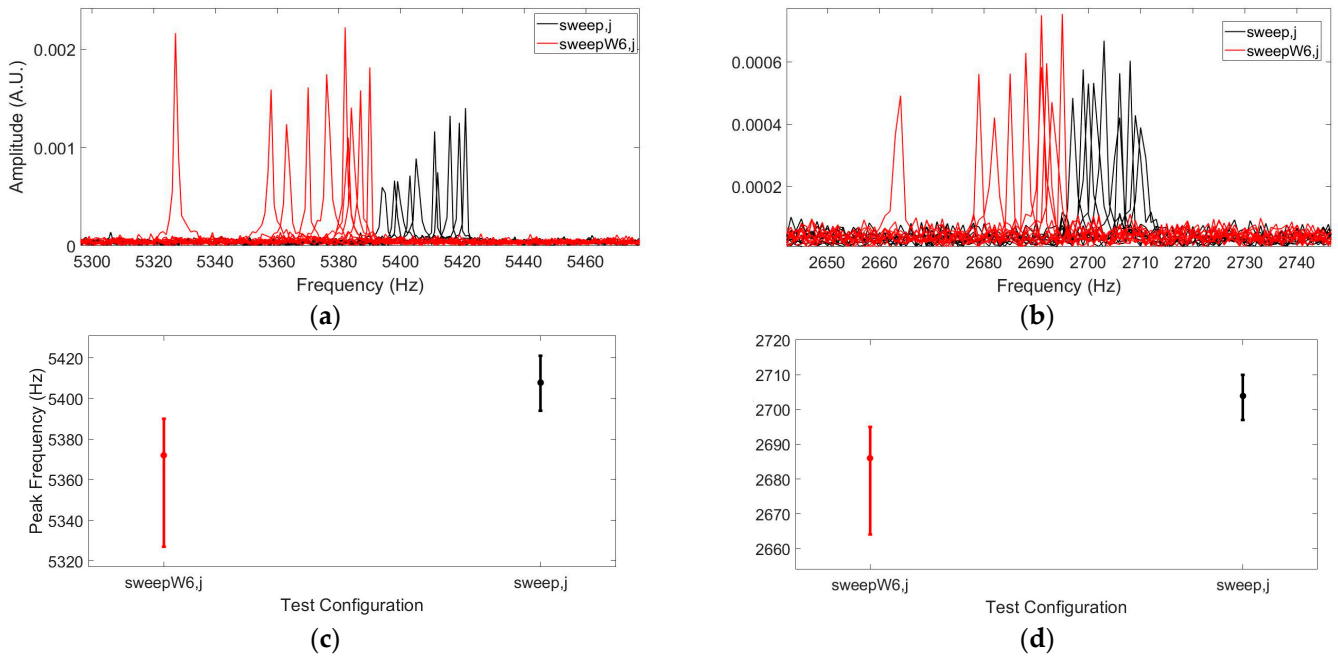


**Figure 11.** Frequency plots of voltage signals obtained via the pick-up coil from a slab vibrating due to frequency sweep excitation without and with mass at W6: (a) peaks in first principal activity region; (b) peaks in second principal activity region; (c) peak dispersion for both configurations in first principal activity region; (d) peak dispersion for both configurations in first principal activity region.

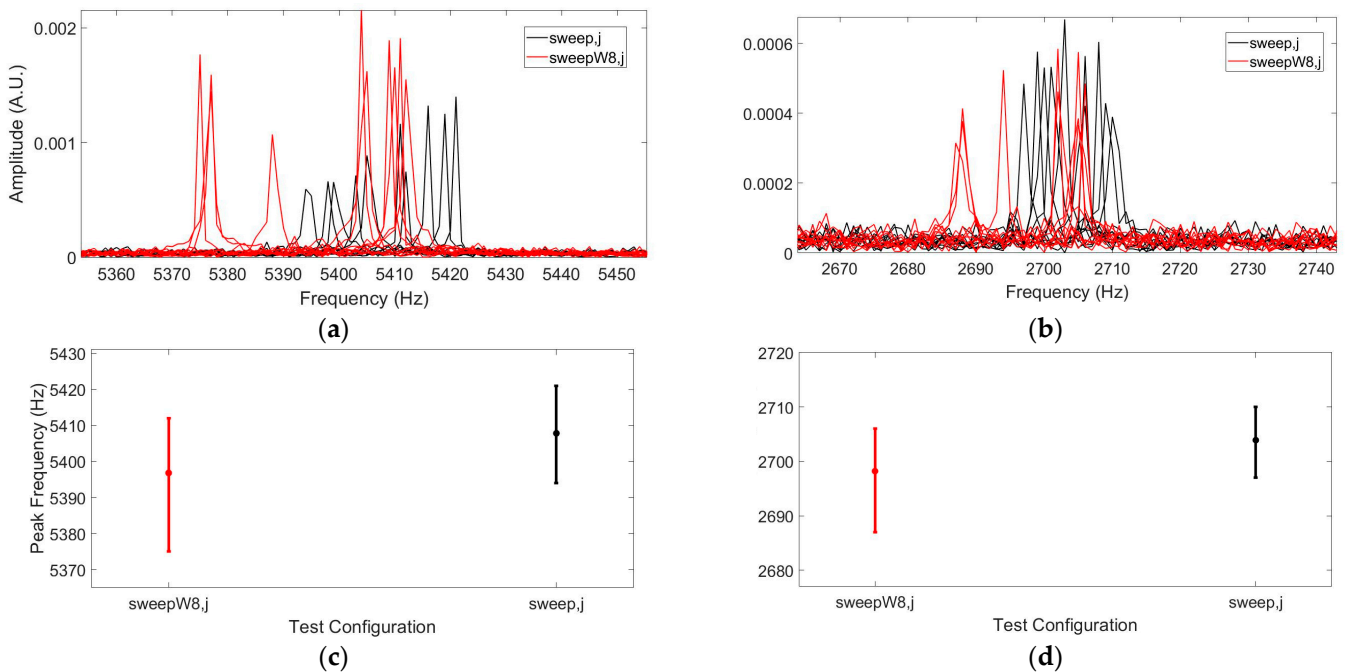


**Figure 12.** Frequency plots of voltage signals obtained via the pick-up coil from a slab vibrating due to frequency sweep excitation without and with mass at W8: (a) peaks in first principal activity region; (b) peaks in second principal activity region; (c) peak dispersion for both configurations in first principal activity region; (d) peak dispersion for both configurations in first principal activity region.

#### 4. Discussion

Results presented in Section 3 are quite promising because they statistically demonstrate that the setup may comfortably detect mass deposition at location W4 when frequency sweeps are used for vibrating the slab. Results presented in the seventh row of Table 2 along with Figure 9 ensure that, even for mass values lower than 0.46 g, there is a comfortable margin for detecting frequency shifts, especially inside the first principal activity region. This confirms that, in terms of sensitivity (see Section 3.1), a vibration profile obtained via frequency sweep excitation was found as the best-case scenario for detecting a mass at W4. Section 3.1 concluded that vibrating the slab at a constant frequency of 180Hz corresponded to the worst-case scenario in terms of sensitivity. This also seemed to be the case when detecting a mass of 0.46 g at W4 because, by looking at the third row of Table 2 and at Figure 7, one realizes that detection margins were considerably slimmer than those obtained when the slab received excitation with frequency sweep profiles. Nonetheless, it is also important to know that, even in the worst case, the proposed setup may still provide acceptable results in terms of mass detection at W4, even though mass value cannot be considerably lower than 0.46 g. When frequency sweeps were used for vibrating the slab, results also seemed to be reasonable in terms of mass detection at location W6. The eighth row of Table 2 and Figure 11 suggest that a mass of 0.46 g may be easily detected from frequency shifts inside both principal activity regions. It is true, however, that detection margins were less significant than those previously obtained for masses located at W4. One could detect mass values lower than 0.46 g, but not by much. These results also point out that the detection effectiveness decreased gradually when the mass was located at a greater distance from the Metglas<sup>®</sup> ribbon. The same reasoning is also valid for a mass accumulated at location W8. Now, looking at the ninth row of Table 2 and Figure 12, one sees that it was not possible to detect mass deposition located so close to the source of vibration, at least when the slab vibrated due to frequency sweeps.

On the contrary, when the slab vibrated at a constant frequency of 180Hz, it seemed that masses of 0.46 g may have been detected at W6 or W8 locations (see fourth and fifth rows of Table 2 and Figures 8 and 9). This is even more surprising, since vibrating the slab at a constant frequency of 180Hz corresponded to the worst-case scenario in Section 3.1. However, a careful examination of Figures 8 and 9 indicates that frequency peaks from tests with a slab loaded at W6 or W8 shifted to higher (instead of lower) with respect to those from tests with unloaded slab. This result does not seem to be in accordance with what is normally experienced in such cases (see, for instance, [22]). A possible explanation, though, may be as follows. Recall that the ultra-thin and, hence, flexible slab is actually an elastic structure that experiences rapid vibrations but of very low amplitude. In the past, various studies considered the special effect of strong mechanical high-frequency excitation causing a flexible structure to apparently “stiffen” [38,39]. There is, obviously, no real stiffening effect in the structure, as if, for instance, extra material had been added to critical locations of the structure. Instead, one may consider that, under specific conditions of high-frequency, low-amplitude vibration, flexible systems may behave as less flexible ones. Specifically, Thomsen in [39] carried out a theoretical and experimental study of a flexible horizontal piano string, clamped on one end and subjected to high-frequency but low-amplitude vibration. Thomsen provided theoretical expressions for *apparent* bending frequencies, which involved the values of standard characteristic frequencies augmented by terms depending on the average effect of the high-frequency excitation. The additional apparent stiffness was not distinguishable from real structural stiffness. More recent studies [40] additionally examined theoretically and experimentally the effect of strong nonlinearities for specific 1-DOF systems in controlling the effective mechanical stiffness.

In essence, this result is quite interesting because it illustrates that, in terms of excitation, faster is not always better when monitoring frequency peaks of flexible structures under low-amplitude vibrations, as was the case in the current study. When the slab vibrated at 180Hz, the experimental findings in Figures 8 and 9 showed that, regardless

of the mass location (W6 or W8), frequency peaks were placed in the same region in the frequency band. It seems that, given the strong excitation, the mass position had no impact on the elastic behavior of the slab. The Kruskal–Wallis test validated this remark, since it was used to solve the hypothesis testing problem (1) when the following datasets were involved, as follows:

- The dataset with peak frequency values from tests at “180HzW6,*j*” configurations;
- The dataset with peaks from test at “180HzW8,*j*” configurations.

The hypothesis testing problem was solved for both principal activity regions, with the Kruskal–Wallis test providing *p*-values equal to 0.96971 ( $H_0$  accepted) for the first and 0.90798 ( $H_0$  accepted) for the second principal activity regions. Hence, placing 0.46 g at either W6 or W8 location had hardly any effect on the apparent stiffness of the loaded slab when the latter vibrated at a (very) low amplitude but rapidly at 180Hz. The overall most effective vibration profile was that relying on frequency sweeps from 30–180Hz, as proposed in Section 3.1.

Another remark is related to the potential use of the Kolmogorov–Smirnov two-sample (instead of Kruskal–Wallis) test for solving the hypothesis testing problem (1). In other words, results on the sensitivity of mass detection at W4, W6, and W8 on the slab surface should hold irrespective of the statistical test used for solving the hypothesis problem (1). Obviously, this remark also depends on how the considered statistical test performs when datasets of a small size (i.e., with limited number of values) are used. As stated in Section 3.2, when using the Kolmogorov–Smirnov two-sample test to solve the hypothesis problem (1) for datasets containing 10 values each, the estimated *p*-values are to be accepted with caution. Massey’s classic paper [41] studied the operational characteristics of the Kolmogorov–Smirnov “goodness-of-fit” test several decades ago. This test is related to statistically evaluating the difference between an empirical and a hypothetical cumulative distribution from available data. Modifications to this test by Khamis [42] aimed specifically at improving the standard test’s power when small to moderate dataset sizes were used. Khamis reported significant improvements (over the standard test) in estimated *p*-values for two examples with datasets of 12 and 9 values, respectively. Even though these papers studied the Kolmogorov–Smirnov goodness-of-fit test (not the two-sample variant), it is reasonable to question the test performance for small datasets.

Consequently, in an effort to verify whether changing the test would lead to different detection results for locations W4, W6, and W8, the hypothesis testing problem (1) was again solved for the same comparisons found in Table 2, but this time using the Kolmogorov–Smirnov two-sample test. Table 3 presents results for cases equivalent to those presented in Table 2. A careful cross-examination of Tables 2 and 3 ensures that, for all comparisons presented in both tables, results are identical in terms of accepted hypothesis. However, a closer look reveals that *p*-values estimated via the Kolmogorov–Smirnov test are somewhat affected by the low number of data points (equal to 10) for each dataset. For instance, Figure 10 presents frequency peaks resulting from test runs at “sweep,*j*” (in black) and “sweepW4,*j*” (in red) configurations inside the first and second principal activity regions. The distance between sets from loaded and unloaded configurations inside the first principal activity region was different to that of the corresponding sets in the second principal activity region. Yet, the respective *p*-values estimated via Kolmogorov–Smirnov tests were identical and equal to 0.00001888 (seventh row, first and second columns in Table 3). The same comparison via Kruskal–Wallis tests (see seventh row, first and second columns in Table 2) yielded *p*-values of 0.00015262 and 0.00015174 for sets in the first and second principal activity region, respectively. This slight difference better demonstrated the situation presented in Figure 10a,b and probably highlights the fact that when datasets become smaller, the use of Kruskal–Wallis tests may be a better solution. Nonetheless, the conclusions on achieving better detection sensitivity at location W4 when the slab was excited via pulses of sweeping frequency still hold, even when the Kolmogorov–Smirnov test was used.



**Table 3.** Test runs and associated configurations, with statistical hypothesis testing results using Kolmogorov–Smirnov two-sample test.

Configuration for Each Dataset $j = 1, \dots, 10$	$p$ -Value: Accepted Hypothesis First Principal Activity Region 5200–5400Hz	$p$ -Value: Accepted Hypothesis Second Principal Activity Region 2500–2700Hz
180Hz $_j$	$1-H_0$	$1-H_0$
180HzW4 $_j$	0.0068986— $H_1$	0.0068986— $H_1$
180HzW6 $_j$	0.00017012— $H_1$	0.00017012— $H_1$
180HzW8 $_j$	0.00017012— $H_1$	0.00017012— $H_1$
sweep $_j$	$1-H_0$	$1-H_0$
sweepW4 $_j$	0.00001888— $H_1$	0.00001888— $H_1$
sweepW6 $_j$	0.00001888— $H_1$	0.00001888— $H_1$
sweepW8 $_j$	0.31285— $H_0$	0.31285— $H_0$

A final remark is related to how a specific electromagnetic noise from a ringing mobile phone may affect the detection effectiveness of the proposed setup. For this purpose, additional experiments were carried out, as follows:

- One set of 10 test runs with the pick-up coil recording signal while the slab was at rest (hence, pure electromagnetic noise);
- Another set of 10 runs under similar (as above) conditions but with a ringing smartphone now supporting the free end of the slab, as described in Section 2.1.

Recall that when the slab was vibrating, frequency components of the recorded signal were easily distinguishable from pure electromagnetic noise as found in the laboratory environment (see Figure 5). Consequently, if even the standard ambient electromagnetic noise is not affected by interferences from a ringing smartphone, then the detection performance of the proposed setup is not going to be affected. The amplitude dispersion of the frequency peaks for both sets of 10 runs is presented in Figure 13: it is seen that a ringing mobile phone did not significantly affect the frequency content of standard electromagnetic noise inside both principal activity regions. Moreover, the hypothesis testing problem was formulated [as in (1)] to examine whether the two sets followed the same statistical distribution (hypothesis  $H_0$ ) or not (alternative hypothesis  $H_1$ ). The problem was solved at a risk level of  $\alpha = 0.05$  for both principal activity regions using the Kruskal–Wallis test. The resulting  $p$ -values were equal to  $0.44 \gg 0.05$  ( $H_0$  accepted) for the first and  $0.65 \gg 0.05$  ( $H_0$  accepted) for the second principal activity regions. Hence, no major interference from a ringing mobile phone was possible in both regions. The result is plausible, since the frequencies of mobile phone operation are much higher than the range where both principal activity regions are located.

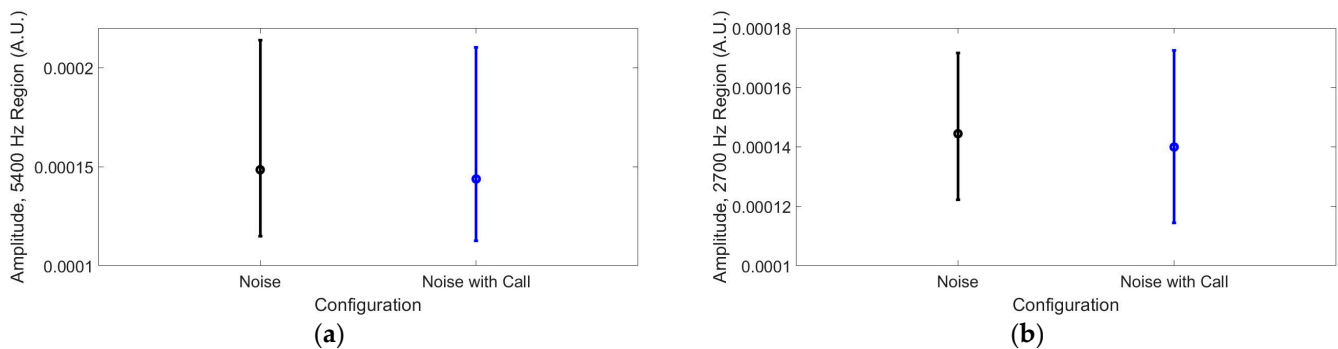


**Figure 13.** Amplitude dispersion of frequency peaks of signals recorded with the slab at rest (i.e., mainly electromagnetic ambient noise), for an idling (in black) or a ringing (in blue) mobile phone: (a) first principal activity region; (b) second principal activity region.

## 5. Conclusions

The development and optimization of a setup utilizing the magnetoelastic characteristics of Metglas<sup>®</sup> ribbons for detecting the accumulation of substances/agents inside a monitored site are presented. The main parts include a short but thin and flexible polymer slab, fixed as a cantilever on one end, with the opposite end receiving support and excitation from a cellular phone. A short Metglas<sup>®</sup> ribbon is attached on the slab's surface near the cantilever end. A pick-up coil suspended above the ribbon receives in a contact-less manner the magnetic flux created when the slab and ribbon vibrate due to the cellular phone being operated. Spectral characteristics of the resulting voltage depend on the vibration dynamics of the slab. These, in turn, are affected by the mass of substances accumulating on its surface. Thus, monitoring specific spectral characteristics (frequency shifts) of the voltage signal allows for verifying the presence of a mass on the slab surface. The proof of concept of the setup was presented in a previous work, but the current study takes the concept to maturity by using extended testing to statistically evaluate its performance/effectiveness and define its operational strengths and limitations. It was concluded that, when vibrating due to an optimal excitation signal (pulses at frequency sweeps from 30–180Hz), the setup may easily detect 0.46 g of a mass at its most sensitive position (that near the clamp). Most interestingly, the statistical methodology used implies that detection margins at that position are quite large, meaning that masses even significantly less than 0.46 g are potentially detectable. On the other hand, if the user inadvertently selects the worst-case excitation scenario (constant frequency of 180Hz), the setup may still provide detection results at the most sensitive position but the sensitivity is somewhat compromised. Further work involves proposing improvements on the pick-up coil circuit used via the development of suitable strategies for upgrading its sensitivity without resorting to costly solutions.

**Author Contributions:** Conceptualization, D.D.; methodology, D.D. and I.K.; software, I.K.; validation, I.K.; formal analysis, D.D. and I.K.; investigation, D.D.; resources, D.D.; data curation, I.K.; writing—original draft preparation, D.D.; visualization, I.K. and D.D.; supervision, D.D.; project administration, D.D. All authors have read and agreed to the published version of the manuscript.

**Funding:** This research received no external funding.

**Data Availability Statement:** Data are available on a personal need basis by contacting the corresponding author of the published article and upon agreement with the authors.

**Acknowledgments:** The second author (D.D.) wishes to thank D.E. Mouzakis for providing the Metglas<sup>®</sup> film.

**Conflicts of Interest:** The authors declare no conflicts of interest.

## References

1. Michalski, S. Care and preservation of collections. In *Running a Museum: A Practical Handbook*; Boylan, P.J., Ed.; ICOM–International Council of Museums, Maison de l'UNESCO: Paris, France, 2004; pp. 51–90.
2. Querner, P. Insect Pests and Integrated Pest Management in Museums, Libraries and Historic Buildings. *Insects* **2015**, *6*, 595–607. [[CrossRef](#)] [[PubMed](#)]
3. Pinniger, D. Past, present and future: Changes in status and distribution of museum insect pests. In *Integrated Pest Management (IPM) in Museums, Archives and Historic Houses—Proceedings of the International Conference in Vienna, Vienna, Austria, 5–7 June 2013*; Querner, P., Pinniger, D., Hammer, A., Eds.; 2013; pp. 20–30. Available online: [https://museumpests.net/wp-content/uploads/2016/03/Vienna\\_IPM\\_1SM.pdf](https://museumpests.net/wp-content/uploads/2016/03/Vienna_IPM_1SM.pdf) (accessed on 20 October 2024).
4. Le Bras, Y.; Greneche, J.M. Magneto-elastic resonance: Principles, modeling and applications. In *Resonance*; Awrejcewicz, J., Ed.; IntechOpen: London, UK, 2017. [[CrossRef](#)]
5. Hristoforou, E.; Ktena, A. Magnetostriction and magnetostrictive materials for sensing applications. *J. Magn. Magn. Mater.* **2007**, *316*, 372–378. [[CrossRef](#)]
6. Grimes, C.A.; Roy, S.C.; Cai, Q. Theory, instrumentation and applications of magnetoelastic resonance sensors: A review. *Sensors* **2011**, *11*, 2809–2844. [[CrossRef](#)]
7. Ren, L.; Yu, K.; Tan, Y. Applications and advances of magnetoelastic sensors in biomedical engineering: A review. *Materials* **2019**, *12*, 1135. [[CrossRef](#)]

8. Lopes, A.C.; Sagasti, A.; Lasheras, A.; Muto, V.; Gutiérrez, J.; Kouzoudis, D.; Barandiarán, J.M. Accurate Determination of the Q Quality Factor in Magnetoelastic Resonant Platforms for Advanced Biological Detection. *Sensors* **2018**, *18*, 887. [[CrossRef](#)]
9. Grimes, C.A.; Jain, M.K.; Singh, R.S.; Cai, Q.; Mason, A.; Takahata, K.; Gianchandani, Y. Magnetoelastic microsensors for en-vinronmental monitoring. In Proceedings of the 14th IEEE International Conference on Micro Electro Mechanical Systems (MEMS), Interlaken, Switzerland, 25 January 2001; pp. 278–281. [[CrossRef](#)]
10. Baimpos, T.; Boutikos, P.; Nikolakakis, V.; Kouzoudis, D. A polymer-Metglas sensor used to detect volatile organic com-pounds. *Sens. Actuator A Phys.* **2010**, *158*, 249–253. [[CrossRef](#)]
11. Atalay, S.; Izgi, T.; Kolat, V.S.; Erdemoglu, S.; Orhan, O.I. Magnetoelastic humidity sensors with TiO<sub>2</sub> nanotube sensing layers. *Sensors* **2020**, *20*, 425. [[CrossRef](#)]
12. Grimes, C.A.; Kouzoudis, D. Remote query measurement of pressure, fluid-flow velocity and humidity using magnetoelastic thick-film sensors. *Sens. Actuators A Phys.* **2000**, *84*, 205–212. [[CrossRef](#)]
13. Grimes, C.A.; Kouzoudis, D.; Dickey, E.C.; Qian, D.; Anderson, M.A.; Shahidian, R.; Lindsey, M.; Green, L. Magnetoelastic sensors in combination with nanometer-scale honey combed thin film ceramic TiO<sub>2</sub> for remote query measurement of humidity. *J. Appl. Phys.* **2000**, *87*, 5341–5343. [[CrossRef](#)]
14. Samourganidis, G.; Nikolaou, P.; Gkovosdis-Louvaris, A.; Sakellis, E.; Blana, I.M.; Topoglidis, E. Hemin-modified SnO<sub>2</sub>/Metglas electrodes for the simultaneous electrochemical and magnetoelastic sensing of H<sub>2</sub>O<sub>2</sub>. *Coatings* **2018**, *8*, 284. [[CrossRef](#)]
15. Dimogianopoulos, D.G. Sensors and energy harvesters utilizing the magnetoelastic principle: Review of characteristic applications and patents. *Recent Pat. Elec. Eng.* **2012**, *5*, 103–119. [[CrossRef](#)]
16. Sagasti, A.; Gutiérrez, J.; Lasheras, A.; Barandiarán, J.M. Size Dependence of the Magnetoelastic Properties of Metallic Glasses for Actuation Applications. *Sensors* **2019**, *19*, 4296. [[CrossRef](#)] [[PubMed](#)]
17. Skinner, W.S.; Zhang, S.; Guldberg, R.E.; Ong, K.G. Magnetoelastic Sensor Optimization for Improving Mass Monitoring. *Sensors* **2022**, *22*, 827. [[CrossRef](#)] [[PubMed](#)]
18. Atalay, S.; Inan, O.O.; Kolat, V.S.; Izgi, T. Influence of Ferromagnetic Ribbon Width on Q Factor and Magnetoelastic Resonance Frequency. *Acta Phys. Pol. A* **2021**, *139*, 159–163. [[CrossRef](#)]
19. Ren, L.; Cong, M.; Tan, Y. An Hourglass-Shaped Wireless and Passive Magnetoelastic Sensor with an Improved Frequency Sensitivity for Remote Strain Measurements. *Sensors* **2020**, *20*, 359. [[CrossRef](#)]
20. Saiz, P.G.; Gandia, D.; Lasheras, A.; Sagasti, A.; Quintana, I.; Fdez-Gubieda, M.L.; Gutiérrez, J.; Arriortua, M.I.; Lopes, A.C. Enhanced mass sensitivity in novel magnetoelastic resonators geometries for advanced detection systems. *Sens. Actuators B Chem.* **2019**, *296*, 126612. [[CrossRef](#)]
21. Saiz, P.G.; Porro, J.M.; Lasheras, A.; Fernández de Luis, R.; Quintana, I.; Arriortua, M.I.; Lopes, A.C. Influence of the magnetic domain structure in the mass sensitivity of magnetoelastic sensors with different geometries. *J. Alloys Compd.* **2021**, *863*, 158555. [[CrossRef](#)]
22. Saiz, P.G.; Porro, J.M.; Lasheras, A.; Fernández de Luis, R.; Quintana, I.; Arriortua, M.I.; Lopes, A.C. Magnetoelastic Resonance-Sensors: Principles, Applications, and Perspectives. *ACS Sens.* **2022**, *7*, 1248–1268. [[CrossRef](#)]
23. Dimogianopoulos, D.G.; Mouzakis, D.E. A Versatile Interrogation-Free Magnetoelastic Resonator Design for Detecting Deterioration-Inducing Agents. In Proceedings of the 1st International Conference on Structural Damage Modelling and Assessment, Ghent University, Belgium, 4–5 August 2020; Abdel Wahab, M., Ed.; Lecture Notes in Civil Engineering. Springer: Singapore, 2021; Volume 110. [[CrossRef](#)]
24. Sultana, R.G.; Davrados, A.; Dimogianopoulos, D. Evaluating contact-less sensing and fault diagnosis characteristics in vibrating thin cantilever beams with MetGlas<sup>®</sup> 2826 MB ribbon. *Vibration* **2024**, *7*, 36–52. [[CrossRef](#)]
25. Dimogianopoulos, D.G.; Charitidis, P.J.; Mouzakis, D.E. Inducing damage diagnosis capabilities in carbon fiber reinforced polymer composites by magnetoelastic sensor integration via 3D printing. *Appl. Sci.* **2020**, *10*, 1029. [[CrossRef](#)]
26. Dimogianopoulos, D.G.; Mouzakis, D.E. Nondestructive Contactless Monitoring of Damage in Joints between Composite Structural Components Incorporating Sensing Elements via 3D-Printing. *Appl. Sci.* **2021**, *11*, 3230. [[CrossRef](#)]
27. Samourganidis, G.; Kouzoudis, D. A pattern matching identification method of cracks on cantilever beams through their bending modes measured by magnetoelastic sensors. *Theor. Appl. Fract. Mech.* **2019**, *103*, 102266. [[CrossRef](#)]
28. Samourganidis, G.; Kouzoudis, D. Characterization of magnetoelastic ribbons as vibration sensors based on the measured natural frequencies of a cantilever beam. *Sens. Actuator A Phys.* **2020**, *301*, 111711. [[CrossRef](#)]
29. Samourganidis, G.; Kouzoudis, D. Magnetoelastic Ribbons as Vibration Sensors for Real-Time Health Monitoring of Rotating Metal Beams. *Sensors* **2021**, *21*, 8122. [[CrossRef](#)]
30. Tapeinos, C.I.; Kamitsou, M.D.; Dassios, K.G.; Kouzoudis, D.; Christogerou, A.; Samourganidis, G. Contactless and Vibration-Based Damage Detection in Rectangular Cement Beams Using Magnetoelastic Ribbon Sensors. *Sensors* **2023**, *23*, 5453. [[CrossRef](#)]
31. Kouzoudis, D.; Samourganidis, G.; Tapeinos, C.I. Contactless Detection of Natural Bending Frequencies using Embedded Metallic-Glass Ribbons inside Plastic Beams made of 3-D Printing. *Recent Prog. Mater.* **2021**, *3*, 010. [[CrossRef](#)]
32. García-Arribas, A.; Gutiérrez, J.; Kurlyandskaya, G.V.; Barandiarán, J.M.; Svalov, A.; Fernández, E.; Lasheras, A.; de Cos, D.; Bravo-Imaz, I. Sensor Applications of Soft Magnetic Materials Based on Magneto-Impedance, Magneto-Elastic Resonance and Magneto-Electricity. *Sensors* **2014**, *14*, 7602–7624. [[CrossRef](#)]
33. Rao, S.S. *Mechanical Vibrations*, 5th ed.; Prentice Hall: Upper Saddle River, NJ, USA, 2011; pp. 721–734.
34. Zar, J.H. *Biostatistical Analysis*, 5th ed.; Prentice Hall: Upper Saddle River, NJ, USA, 2010.

35. Hoffman, J.I.E. *Basic Biostatistics for Medical and Biomedical Practitioners*, 2nd ed.; Elsevier Science: Amsterdam, The Netherlands, 2019; ISBN 978-0-12-817084-7. [[CrossRef](#)]
36. Getting Started with the Kruskal Wallis-Test | UVA Library. Available online: <https://library.virginia.edu/data/articles/getting-started-with-the-kruskal-wallis-test> (accessed on 23 September 2024).
37. Kstest2, Two-Sample Kolmogorov-Smirnov Test. Available online: <https://www.mathworks.com/help/stats/kstest2.html> (accessed on 23 September 2024).
38. Thomsen, J.J. Some general effects of strong high-frequency excitation: Stiffening, biasing and smoothening. *J. Sound Vib.* **2002**, *253*, 807–831. [[CrossRef](#)]
39. Thomsen, J.J. Theories and experiments on the stiffening effect of high-frequency excitation for continuous elastic systems. *J. Sound Vib.* **2003**, *260*, 117–139. [[CrossRef](#)]
40. Thomsen, J.J.; Ebbenhøj, K.L. Strong nonlinearity and external high-frequency forcing for controlling effective mechanical stiffness: Theory and experiment. *Nonlinear Dyn.* **2023**, *111*, 6985–7003. [[CrossRef](#)]
41. Massey, F.T. The Kolmogorov-Smirnov test for goodness of fit. *J. Am. Stat. Assoc.* **1951**, *46*, 68–78. [[CrossRef](#)]
42. Khamis, H.J. The two-stage  $\delta$ -corrected Kolmogorov-Smirnov test. *J. Appl. Stat.* **2000**, *27*, 439–450. [[CrossRef](#)]

**Disclaimer/Publisher’s Note:** The statements, opinions and data contained in all publications are solely those of the individual author(s) and contributor(s) and not of MDPI and/or the editor(s). MDPI and/or the editor(s) disclaim responsibility for any injury to people or property resulting from any ideas, methods, instructions or products referred to in the content.